Environmental Science

http://www.aimspress.com/journal/environmental

AIMS Environmental Science, 5(5): 315–339.
DOI: 10.3934/environsci.2018.5.315
Received: 21 July 2018
Accepted: 26 October 2018
Published: 14 November 2018

Research article

Simulations of vehicle-induced mixing and near-road aerosol microphysics using computational fluid dynamics

Satbir Singh[1,*], **Peter J. Adams**[2,3] **and Albert A. Presto**[1]

[1] Department of Mechanical Engineering, Carnegie Mellon University, 5000 Forbes Avenue, Pittsburgh, PA 15213, USA

[2] Department of Civil and Environmental Engineering, Carnegie Mellon University, 5000 Forbes Avenue, Pittsburgh, PA 15217, USA

[3] Department of Engineering and Public Policy, Carnegie Mellon University, 5000 Forbes Avenue, Pittsburgh, PA 15217, USA

* **Correspondence:** Email: satbirs@andrew.cmu.edu; Tel: +14122683263; Fax: +14122683348.

Abstract: Understanding the fate of ultrafine particles (UFP), especially from combustion sources, is essential to assess their impact on health and climate. Here, we present simulations of the behavior of UFP in the near-roadway environment (up to 300 m downwind) based on a model with coupled computational fluid dynamics (CFD) and aerosol microphysics. It is found that vehicle-induced mixing (VIM) caused by the combined effect of vehicle wake formation and production of turbulent kinetic energy plays an important role in downwind dilution of pollutants. Various methodologies for simulating VIM are explored, and a computationally efficient approach based on an effective roughness length for vehicle-induced mixing is proposed. Whereas the coagulation behavior of ultrafine particles is relatively well understood, condensation and/or evaporation can have equally large or larger impacts on the number and sizes of particles downwind of a roadway. Through a set of sensitivity simulations, we show that the particle losses are potentially significant via evaporation but depend strongly on several parameters or processes that are poorly understood and difficult to fully constrain for on-road traffic using measurements: the volatility distribution of organic species and gas-phase concentrations of semi-volatile organics.

Keywords: traffic pollution; near-roadway; CFD simulations; vehicle-induced mixing; ultrafine particles

1. Introduction

Traffic-related particulate matter (PM) impacts human health through direct exposure [1] and influences climate through its role in cloud formation and radiative forcing [2–4]. Most existing environmental and emission standards are based on $PM_{2.5}$ (<2.5 μm) mass concentration, while the total number is often dominated by the ultrafine particles (UFP), particles smaller than 100 nm in diameter. Due to their small size and high ambient number concentrations, UFP may have distinct health and climate impacts from $PM_{2.5}$ as a whole, which is dominated by particles larger than 100 nm. Epidemiological studies have suggested increased risk for health effects for populations that live near roadways, which may not be due to $PM_{2.5}$ mass, since near-road mass concentrations are elevated only by 25–50% compared to urban background levels [5]. On the other hand, UFP have 3–5 times higher number concentrations near roadways [6, 7]. For roadways passing through urban areas, vehicles are a major source of UFP. Elevated concentrations of UFP have been linked to many adverse health effects [8]. Because of clearly identified adverse health effects of particulate matter, understanding on-road UFP emissions and the physicochemical processes governing their near-roadway concentration profiles is critical to gaining a better knowledge of UFP exposures to populations living near major roadways.

Aerosol particles can directly scatter and absorb solar radiation, producing a net cooling effect on the atmosphere [9], and can indirectly affect the climate system by acting as cloud condensation nuclei (CCN). The direct effects are mostly related to the mass, water absorption ability, and optical properties [9–12]. Among these, mass of PM emissions from many combustion systems is relatively well constrained [13–19] making it somewhat easier to quantify the direct effects of PM. In contrast, the indirect effects cannot be easily quantified due to large uncertainties in constraining the growth of emitted UFP to CCN sizes (>100 nm), their subsequent atmospheric chemical aging, uncertainty in optical properties, and the formation of cloud droplets. Emissions of traffic-related particle number and the accompanying particle size distribution are also not well constrained. Most three-dimensional (3D) atmospheric-aerosol models parameterize PM number from source measurements of PM mass, and do not account for the effects of sub-grid scale particle microphysics on particle size distributions [2, 20]. Sub-grid scale here refers to the phenomena occurring at scales smaller than the CFD computational grid size. For large scale atmospheric models CFD grid cells are very large such that near-source particle microphysics occurring within few hundred meters is often ignored. For traffic-related emissions, the sub-grid scale microphysics will be active within few hundred meters from the roadway. A simple method was proposed to account for sub-grid scale effects of coagulation on the particle size distribution emitted into regional or global chemical transport models but did not consider condensation or evaporation of organics, a process expected to be important in the near roadway environment for traffic emissions [21]. It was found that if sub-grid scale (defined as below 500 km in that work) coagulation is taken into consideration, the size distribution used in the global chemical transport models (CTMs) will deviate substantially from the emitted distribution. Therefore, better knowledge of both emitted size distributions and understanding of sub-grid scale microphysics are important for providing scientific inputs to regional-scale CTMs and global climate models. Simulations of near-roadway microscale environment can potentially bridge the gap between the source-level emission inventories and coarse-scale global CTM simulations.

Once emitted from the vehicle tailpipe, aerosol particles go through very rapid dilution in the

near-tailpipe region, vehicle-induced mixing in the immediate vicinity of the roadway, and slower atmospheric dilution away from the roadway [22–28]. Measurements suggest that CO concentration can decrease by almost 50% within first 20 meters from the edge of the roadway [29]. Accounting for motion of the vehicles on the roadway was found to be critical to obtain accurate predictions of rapid near-roadway dilution using CFD [22, 23]. On top of the atmospheric dilution, complex physiochemical phenomena such as nucleation, evaporation/condensation, coagulation can all take place simultaneously modifying the characteristics of aerosol particles [30]. Measurements taken near a major highway indicate that particles smaller than 20 nm are mostly semi-volatile, while particles larger than 20 nm contain both volatile and non-volatile matter [31]. As these semi-volatile particles are transported away from the roadway, they can coagulate to form larger particles, grow due to condensation or shrink due to evaporation. Near-roadway observations have suggested that particles can be lost due to aerosol microphysics, particularly evaporation and coagulation. Their relative roles, however, are not yet fully understood and quantified. In the presence of barriers such as vegetation and man-made structures, downwind concentration profiles can be further modified either due to re-routing of the flow around structures or deposition on vegetation [32–37].

Predictions provided by CFD simulations can be useful to understand near-roadway exposure and associated controls, and to provide better inputs to the CTM models by accounting for near-roadway processing of tailpipe emissions. The regional scale models are not appropriate due to lack of turbulence parameterization available in these models at the microscale of the near-roadway environment and also due to nonlinear processes that are not well quantified using average concentrations from relatively coarse CTM grid cells. The plume models based on Gaussian dispersion do not account for complex nature of the terrain, and have to often rely on experimental measurements or CFD simulations for quantification of vehicle-induced mixing. On-road vehicle motion and turbulence generation was simulated to provide better inputs for a near-roadway Gaussian plume model, which was used to predict dispersion of vehicle emitted CO [22]. Direct application of CFD simulations to study pollution dispersion in the atmosphere has been limited mostly to passive transport in street canyons [38, 39], around physical barriers [37, 40, 41], and urban setup with simplified representation of buildings [42]. CFD has been used to simulate passive dilution of CO near two different roadways without accounting for aerosol microphysics [23]. It was concluded that CFD simulations provided better predictions of dilution compared to the plume models. There have also been attempts to understand the chemical transformation of pollutants in the near-roadway environment [43, 44].

Although CFD simulations are better suited than plume models for providing more detailed spatio-temporal evolution of UFP, to date, there have been only a handful of CFD studies of aerosol transport and microphysics in the near-roadway environment [30, 45]. Their role has been limited primarily due to computational cost. Recently, CFD model was used to simulate physiochemical evolution of aerosol emitted by 6 moving vehicles on a roadway [30]. To reduce computational cost researchers simulated a two-way traffic scenario with only one-way traffic in the model. In their simulations, the total number of computational cells was 0.9 million. The computational cell size became almost equal to the vehicle size within about 20 m from the roadway due a large expansion ratio of the grid [30]. Such a large expansion ratio of the grid is not recommended to limit numerical discretization errors. To address the computational cost of full-scale simulations, a multi-scale-structure approach was proposed to decouple on-road simulations from near-roadway

simulations [45]. In this approach, CFD simulations for the entire roadway were performed with 30 vehicles by decoupling it from the near-roadway domain. The outputs of the on-road simulations were used as inputs for the near-roadway simulations by averaging concentrations over the entire on-road computational domain. In the multi-scale-structure approach [45], the on-road computational domain was divided into 3 million computational cells, resulting in only 100,000 cells per vehicle. But as discussed by the same researchers [46], nearly 3 million cells per vehicle are needed to obtain accurate predictions of turbulent kinetic energy produced by the moving vehicles. Therefore, there remains a need to find methods that simulate vehicle-induced mixing in an accurate and efficient manner.

In the present work, simulations are performed to investigate the impact of dilution and aerosol microphysics on the fate of traffic-emitted particles in the near-roadway environment. Fully coupled turbulent flow and aerosol microphysics simulations are performed for a major roadway carrying light- and heavy-duty vehicles. A new approach to simulate vehicle-induced mixing is investigated, without fully resolving the turbulent boundary layer near the vehicle surface. Impact of atmospheric dilution, microphysical processes, and vehicle emissions on UFP characteristics in the near-roadway environment is discussed. It should be mentioned here that the goal of this research is not to compare model predictions with a specific set of near-roadway measurements, but rather to investigate on-road and near-roadway dilution and microphysics for traffic conditions closely relevant to real-world conditions. Therefore, the input data used in the model, specifically at the vehicle tailpipe, is borrowed from multiple measurements. Measurements of particle concentration made in one study are shown for reference [26].

2. Computational model

In this work, a model for aerosol microphysics accounting for particle coagulation, and condensation/evaporation of semi-volatile organics is integrated into a commercial CFD code "CONVERGE" [47] for simulations of UFP in the near-roadway environment. In CONVERGE, a fully-implicit time differencing Pressure Implicit with Splitting of Operators (PISO) algorithm [48] is used for velocity and pressure coupling. A second-order non-weighted central differencing scheme is used to approximate all spatial derivatives. However, in order to aid the numerical stability of the solution, the numerical scheme is switched to first order upwind in the regions of the computational domain where the velocity or density fields become non-monotonic [47]. Reynolds-Averaged Navier-Stokes (RANS) technique is used for predictions of turbulence. In this work, the well-known k-ϵ model was employed. Formulation of RANS transport equations for mass, momentum, energy, and aerosol particles is provided in the Supplemental document. Additional details of numerical schemes available in CONVERGE can be obtained from reference [47]. The aerosol microphysics is incorporated into the code using user defined functions (UDFs).

Aerosol microphysics

To account for the aerosol microphysical processes of coagulation and condensation/evaporation, TwO-Moment Aerosol Sectional (TOMAS) microphysics model of Adams and Seinfeld is used [20]. The algorithms used in the TOMAS model are adaptations of cloud microphysics algorithms [49, 50] to aerosol processes. The TOMAS model solves for two independent moments of the aerosol size

distribution for each size bin or category. The two moments are the aerosol number density and the mass density. The number and mass distributions are discretized into 15 bins. As discussed in [51], mass quadrupling is assumed between neighboring bins, resulting in the smallest particle size of 0.65 nm and the largest particle size of 425 nm. More details of the TOMAS numerical algorithms can be found in [20].

Aerosol particles are assumed to be comprised of three components including elemental carbon (EC) and two surrogate components to represent the suite of semi-volatile organic compounds (OC). Particle emissions from diesel engines also contain sulfur, but the role of sulfur is generally limited primarily to nucleation of new particles. Since the nucleation process itself was not simulated here as discussed in following section, sulfur was not considered in the simulations. The two-component OC model has been previously validated for predicting partitioning of the semi-volatile organic carbon [52] for wood stove and diesel engine combustion, and has been successfully used to predict particle evolution in a lab-scale dilution sampler [53]. Therefore, the two-component model is used in this work to predict condensation/evaporation of OC onto existing particles. Component 1 has molecular weight (MW) of 282 g/mole and saturation concentration (C*) of 500 $\mu g/m^3$, while component 2 has MW of 394 g/mole and saturation concentration (C*) of 2 $\mu g/m^3$ at temperature of 298 K. The saturation concentrations at 298 K were adjusted to account for Kelvin effect using surface tension of 0.03 N/m [54]. These two components will be referred to as OC500 and OC2 in the rest of the paper. With these two components, the model gave reasonably good predictions of OC gas-particle partitioning using 0.25–0.75 and 0.40–0.60 mass fractions of the two components for gasoline and diesel vehicle emissions, respectively, when compared with vehicle emissions data [55, 56]. In the present simulations, OC2 component is primarily responsible for mass transfer between the gas and particle phases, while OC500 remains in the gas phase. Nucleation and dry deposition are ignored in the model.

3. Computational setup

Computational setup is designed to replicate traffic conditions on Interstate 710 (I-710) reported in [26] during January 2002. Size of the computational domain is 380 m in the direction of the wind (along x-axis), which is crosswise to the traffic, 40 m along the road (along z-axis), and 40 m in the vertical direction (along y-axis). Vehicle configuration shown in Figure 1 is similar to the one used in [23]. The highway is 26 m wide including a 3 m wide median with a total of 8 lanes, 4 in each direction. A total of 6 gasoline vehicles are placed on the interior lanes while the 2 diesel trucks are placed in the outer lanes, representing a mix of 75% gasoline vehicles and 25% heavy-duty diesel trucks [26]. The total traffic count was 12,180 vehicles per hour [26].

An octree meshing strategy is used in CONVERGE for local grid refinement. The computational grid is guaranteed to conform to the geometry by allowing polyhedral cell shapes near the boundary surfaces. For reference, computational grid on two one-dimensional slices of the computational domain is shown in Figure 1. The grid becomes gradually coarser away from the vehicles to obtain a total of 1.7 million cells in the entire computational domain. However, even such a large number of grids cells is not adequate to resolve the velocity boundary layer on the vehicle surface. Indeed, it was shown that nearly 3 million cells per vehicle are needed to obtain accurate predictions of turbulent kinetic energy produced by the moving vehicles [46]. For simulation of 8 vehicles moving on a highway,

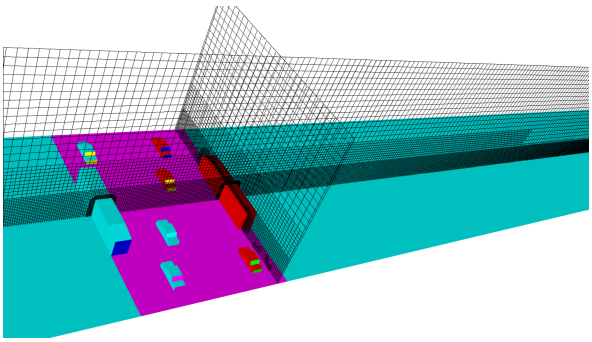

Figure 1. Computational domain, vehicle configuration, and mesh distribution for California highway I-710 site located in Los Angeles [23, 26].

nearly 24 million cells would be needed making the simulations impractical, especially in the presence of aerosol microphysics. But only 1.06 million cells were used for similar flow configuration in one study [23] and 0.9 million cells were used for simulating 6 moving vehicles in another study [30]. As will be discussed later, with the surface roughness used in [23], our model under-predicts turbulence generation on the road; therefore, vehicle surface roughness is adjusted to match with an available experimental parameterization for vehicle-induced turbulent kinetic energy [57]. In our simulations, the maximum value of y^+ on the surface of the vehicles was about 4000. The standard law-of-the-wall model with roughness length was employed to predict wall-shear stress at the surface of the vehicles.

Initial and boundary conditions

At the start of the simulation, the flow field is initialized with a zero velocity. The gas-phase composition is initialized as pure air at temperature of 298 K and pressure of 1 bar. The aerosol particle concentration is also initialized to zero. The boundary conditions for mass, momentum, and energy equations are given in Table 1. For all solid surfaces, temperature is fixed at 298 K, and no-slip boundary condition along with the law-of-the-wall and surface roughness models are used for turbulence. Motion of vehicles is simulated using no-slip velocity boundary condition at the solid walls. A velocity of 25 m/s is specified on all surfaces of each vehicle (along z-axis) to simulate an average vehicle speed of 55 mph. Free shear or zero shear stress boundary condition is applied at the top boundary, and zero-gradient boundary condition is applied at the right boundary for outflow. Periodic boundary conditions are used on two ends of the road which translates into a road of infinite length with repeatable traffic pattern.

A fully developed neutral atmospheric boundary layer (ABL) wind velocity profile and turbulence parameters consistent with the $k - \epsilon$ turbulence model are specified (along x-axis) at the inlet of the computational domain. Following the procedure recommended in [58], friction velocity u^* is estimated using wind speed measurements at the reference location as following:

$$u^* = \kappa U_r \left[ln\left(\frac{z_r}{z_o}\right)\right]^{-1} \tag{3.1}$$

where $U_r = 1.2$ m/s is the wind velocity at the reference height of $z_r = 10$ m measured near I-710 highway [26]. The parameter z_o is the ground surface roughness length taken to be 0.01 m in this

Table 1. Boundary conditions for gasoline and diesel vehicles. All emission rates are given on per vehicle basis.

	Gasoline vehicle	**Diesel vehicle**
Traffic flow (vehicles/hr)	9135	3045
Vehicle speed (m/s)	25	25
CO emission rate (mg/s)	88	88
Particle-phase EC emission rate (mg/s)	0.064	0.77
Particle-phase OC500 emission rate (mg/s)	0	0
Particle-phase OC2 emission rate (mg/s)	0.0037	0.0037
Gas-phase OC500 emission rate (mg/s)	0.0025	0.342
Gas-phase OC2 emission rate (mg/s)	0.0076	0.513
Particles (≤20 nm) specified at tailpipe exit (particles/s)	2.0×10^{12}	2.0×10^{12}
Particles (>20 nm) specified at tailpipe exit (particles/s)	1.6×10^{10}	1.81×10^{12}

work, and $\kappa = 0.4237$ is the von Karman constant in the $k - \epsilon$ model. The wind velocity as a function of vertical distance z is then calculated as

$$U = \frac{u^* ln[(z + z_o)/z_o]}{\kappa} \tag{3.2}$$

The turbulent kinetic energy k and its dissipation ϵ in the wind are specified using

$$k = \frac{u^{*2}}{\sqrt{C_\mu}} \tag{3.3}$$

$$\epsilon = \frac{u^{*3}}{\kappa z} \tag{3.4}$$

where $C_\mu = 0.09$ is a constant coefficient used in the $k - \epsilon$ model.

Release of gas- and particle-phase emissions into the atmosphere is specified using sources at the tailpipe exit for each vehicle. Carbon monoxide (CO) emissions of 5.8 g/mile (88 mg/s at 55 mph) were specified at tailpipe of each vehicle [59]. Condensation/evaporation of semi-volatile organics is predicted using a two-component volatility basis-set (VBS) model. Emissions of semi-volatile organic carbon (OC) are specified using vehicle measurements made at cruise conditions [55, 56]. For each diesel truck, total gas-phase OC of 75 mg/kgf (milligrams per kilograms of fuel) was emitted, which in the model translates into 0.856 mg/s at vehicle speed of 55 mph (88.5 km/h) and fuel economy of 4.3 miles/gallon (1.828 km/l). Total OC was further split into 40% of OC500 and 60% of OC2 for each diesel vehicle to match volatility distribution measured in [55, 56]. For each gasoline vehicle, total OC of 5.17 mg/kgf or 0.01 mg/s at vehicle speed of 55 mph and fuel economy of 25 miles/gallon (10.628 km/l) was emitted with a split of 25% of OC500 and 75% of OC2. A total of 5.17 mg/kgf OC for each gasoline vehicle was calculated using a weighted average of 26% of pre-LEV (13 mg/kgf), 53% of LEV-I (3.25 mg/kgf), 21% of LEV-II vehicles (0.34 mg/kgf) on I-710.

In the measurements [26], aerosol number distributions are available only in the near-road environment with first measurement location at 17 m from the highway median. The model, however, requires distributions at the tailpipe exit. It was pointed out that the measured distribution for I-710

varied significantly from pass-to-pass and from day-to-day leading to uncertainty in measured data [26]. However, despite the uncertainties, the distributions were consistently bi-modal. Since aerosol distribution at the tailpipe exits of actual vehicles on I-710 was not available, we have taken following approach to obtain distributions that qualitatively represent distributions emitted by the vehicles on I-710.

The shape of the distribution is taken from diesel engine lab experiments reported in [60], as shown in Figure 2. At the tailpipe exit, all particles above 20 nm are assumed to be made of only elemental carbon (EC). As given in Table 1, a total of 0.77 mg/s and 0.064 mg/s of EC is emitted from each diesel and gasoline vehicle, respectively. Particles with diameters ≤20 nm are assumed to be semi-volatile as suggested by measurements near I-710 [31]. In reality, semi-volatile particles are formed in the atmosphere via nucleation just as the hot exhaust gases exit the tailpipe and mix with cooler ambient air. In order to accurately account for nucleation in the simulations, much finer mesh resolution near the tailpipe and reliable nucleation theories are required. As presented in [53], sub-millimeter computational cell size near the tailpipe exit is necessary to predict nucleation in a turbulent jet. Such fine mesh resolution is not feasible in the present study due to computational cost. Also, work presented in [53] and numerous other studies have found available nucleation theories to be imperfect in predicting particle nucleation rate. For example, in order to match the total number concentration in the exhaust of a lab diesel engine, the binary nucleation rate had to be multiplied by an *ad hoc* factor of 25 [53]. Such multiplication factors might be quite different for the real world traffic and for each vehicle. Therefore, in this work, we focus on condensation/evaporation and coagulation microphysics in the near-roadway environment with assumed distributions at the vehicle tailpipe that already account for the effects of nucleation. The nucleation-mode particles (diameter ≤ 20 nm) made of OC2 (lower volatility component) are assumed to exist at the tailpipe exit. When these distributions are initialized at the tailpipes of the vehicles, the total number of particles at the first measurement location (17 m) are predicted to be about 1.5×10^5 cm^3, which is similar to the measurements near I-710 [26]. As shown in Figure 2, the number distribution of the nucleation-mode particles (diameter ≤ 20 nm) is assumed to be the same for diesel and gasoline vehicles as suggested by measurements reported near diesel and gasoline highways [26–28].

The background number distribution near highway I-710 in Los Angeles, CA is taken from [26]. As shown in Table 2, the total number density of background particles upwind of the highway is set to 2.49×10^4 cm^{-3}, with 4.5 μg/m^3 of EC [26] and 0.78 μg/m^3 of OC in the particle phase. The nearest IMPROVE site, which is located outside the urban environment close to the interstate 5 (I-5) was used to obtain the background OC concentration. The OC concentration at this site is likely to be lower than the urban environment. Only OC2 was initialized in the particle phase. To obtain equilibrium between particle- and gas-phase OC in the background, 1.33 μg/m^3 of OC500 and 2.20 μg/m^3 of OC2 were initialized in the gas phase.

4. Results and discussion

Simulations were performed to investigate multiple approaches of modeling vehicle-induced mixing (VIM) of pollutants and to understand the impact of various microphysical processes on evolution of particles downwind of the roadway. For VIM, relative roles of vehicle motion and vehicle-induced turbulence (VIT) are investigated. In this work, VIT refers to the production of TKE

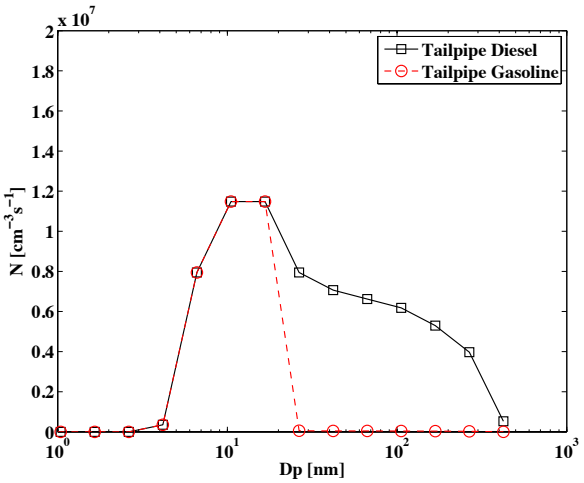

Figure 2. Aerosol particle number distribution specified at the tailpipe of each gasoline and diesel vehicle.

Table 2. Particle-phase and gas-phase composition of background air.

Background particle number density (cm^{-3})	2.49×10^4
Background EC mass density ($\mu g/m^3$)	4.5
Background particle-phase OC2 mass density ($\mu g/m^3$)	0.78
Background particle-phase OC500 mass density ($\mu g/m^3$)	0
Background gas-phase OC2 mass density ($\mu g/m^3$)	2.20
figs Background gas-phase OC500 mass density ($\mu g/m^3$)	1.33

on the roadway, while VIM refers to mixing caused by combined effect of vehicle motion and TKE production. As discussed below, some researchers have proposed methodologies to initialize TKE on the roadway without accounting for vehicle motion. In the present work this approach is referred to as VIT approach. When the vehicles are set in motion, large wakes are created behind each vehicle which lead to wake-enhanced mixing, in addition to turbulent diffusion caused by TKE production. For microphysics, coagulation and condensation/evaporation microphysics are incorporated into the code, and their individual impact on particle evolution is investigated by selectively activating or de-activating each microphysical process. Sensitivity simulations are also performed to investigate the roles of Kelvin effect, and two different gas-phase OC emissions scenarios on particle evolution in the near-roadway environment.

4.1. Predictions of vehicle-induced mixing (VIM) and near-roadway dilution

Moving vehicles generate large wakes and turbulence behind them as they shear through the atmospheric air. Previous research [22, 23, 30] found that it is important to include vehicle-induced mixing in the simulations to obtain correct dilution rates of traffic-emitted pollutants. Predictions of CO [22, 23] were compared with available experimental measurements [26], and it was found that dilution is under-predicted when vehicles are modeled as stationary objects in the model. In the present work, we also find that the dilution rate of CO is under-predicted with stationary vehicles, as

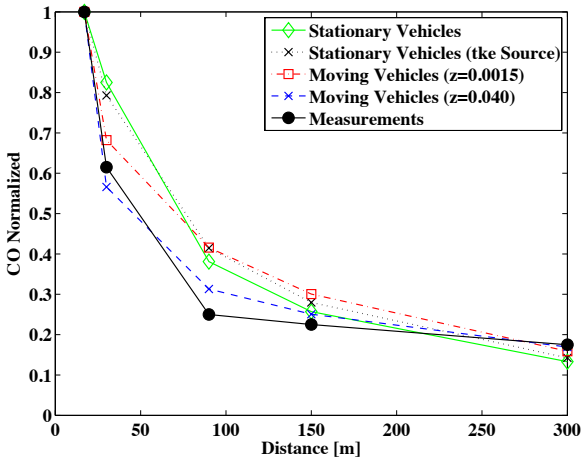

Figure 3. Comparison of measured and predicted normalized CO concentration as a function of distance from highway median for stationary vehicles, stationary vehicles with TKE source (VIT approach), moving vehicles with standard surface roughness (z = 0.0015), and moving vehicles with surface roughness adjusted (z = 0.04) to match TKE predicted by available experimental parameterization [57].

shown in Figure 3. The vehicles are made stationary by setting velocity boundary condition to 0 m/s on the vehicle surface. Stationary vehicles do not generate wakes and turbulence on the roadway, and the mixing is achieved only through interaction of atmospheric cross wind with the vehicles. Figure 3 shows normalized CO concentration as a function of distance from the highway median. Comparison with the experiments is made at 17, 30, 90, 150, and 300 m locations and at height of 1.6 m from the ground [26]. Model predictions are averaged along the length of the road. When the vehicles are simulated as stationary objects, CO emitted on the highway does not go through vehicle-induced mixing (VIM), and there is almost no additional turbulent kinetic energy (TKE) generated on the roadway due to interaction of low velocity atmospheric wind with the vehicle as shown in Figure 4. The TKE on the roadway is essentially equal to the TKE specified in the atmospheric wind, which is 0.04 m^2/s^2. Therefore, as pointed out in [23], a lower CO dilution rate in the simulations is likely because of lack of vehicle generated TKE on the roadway.

Prediction of vehicle generated TKE is computationally expensive due to requirement of finer mesh resolution near the vehicle surface and, hence, smaller simulation timestep size for numerical stability. As pointed out in [46], nearly 3 million cells per vehicle are required to predict TKE production on the roadway. Requirement of such a large computational mesh makes computational modeling impractical and unattractive for real-world applications. Therefore, some researchers have resorted to specifying uniform source of TKE on the roadway with vehicles being stationary [36]. Such an approach may be reasonable if the region of interest in only the roadway, and predictions of TKE profile near the roadway are not critical. In order to illustrate this, a simulation was performed by specifying a uniform TKE of 0.64 m^2/s^2 on the road to match available experimental parameterization of on-road vehicle-induced turbulence [57]. As shown in Figure 3, the dilution rate of CO is under-predicted. Indeed, CO dilution profile is very similar to the one with stationary vehicles. The TKE of 0.64 m^2/s^2 specified on the roadway rapidly dissipates to 0.08 m^2/s^2 at the first measurement location, which is just 4 m

from the edge of the roadway. Therefore, our simulations suggest that specification of a uniform TKE source with stationary vehicles will not provide accurate predictions of dilution rate of pollutants in the near-roadway environment, and that specifying vehicle motion on the roadway is necessary. As discussed below, it is important to specify velocity boundary condition on the vehicle surface to obtain correct trends of vehicle-induced mixing.

Figure 3 includes predictions of CO for two cases in which vehicles were set in motion by specifying a velocity boundary condition of 25 m/s on the surface of all vehicles. For the first case, vehicle surface roughness length was set to 0.0015 m as used in [46]. Surface roughness length is used in the model to mimic rough surfaces, which are not explicitly represented in the model. With the surface roughness length of 0.0015 m, vehicle generated TKE on roadway is 0.25 m^2/s^2 compared to 0.64 m^2/s^2 predicted by the experimental parameterization. We believe that this is due to poor grid resolution at the surface of the vehicles. With vehicle motion along with surface roughness length of 0.0015 m, predictions of CO dilution from 17 m to 30 m location are improved, but the dilution is still under-predicted beyond 30 m location. Improved predictions at 17 m and 30 m locations are primarily due to mixing caused by vehicle wakes. But same level of mixing does not continue into the near-roadway environment, likely due to lack of turbulence, suggested by lack of TKE in the near-roadway environment. A higher grid resolution at the surface of vehicles would have resulted in more on-road TKE generation, and possibly better mixing in the near-roadway environment. But as pointed out earlier, higher grid resolution was not considered here due to prohibitive computational cost. Therefore, in the present work, vehicle surface roughness length in the model was adjusted to 0.04 m to obtain 0.64 m^2/s^2 of TKE on the roadway. With this approach, the TKE at the 17 m location became about 0.4 m^2/s^2, rapidly decreasing to 0.175 m^2/s^2 at the 30 m location as shown in Figure 4. For the new simulation, the normalized CO dilution profile compares much better with the experimental parameterization. These results suggest that dilution of pollutants in the near-roadway environment is governed partly by the bulk motion of vehicles, and partly by vehicle generated TKE that is convected downwind by the atmospheric wind. The use of a large roughness length in our model is partly due to physical justification and partly due to numerical necessity. For the vehicle models used in the present work, real features of the vehicles such as recesses in windows and wind-shields, wipers, side mirrors, grilles, under chassis details etc. are not explicitly represented. All these features are expected to produce more TKE compared to a vehicle with an entirely smooth surface. However, even if those features were explicitly represented in our simulations we believe that the TKE production will still be lower due to coarse mesh at the vehicle surface. Therefore, lack of mesh resolution at the vehicle surface is compensated by numerical adjustment to the roughness length.

Although the approach of numerically adjusting the roughness length can be applied to other traffic configurations, the actual value of the roughness length used for the present simulations may not completely translate to other traffic conditions. To validate the approach for other traffic conditions, we have simulated two more vehicle speeds of 40 mph (64 km/h) and 70 mph (113 km/h) without changing the vehicle configuration in the computational setup. Predictions of our simulations are compared with the predictions of the available experimental parameterization [57]. For the 40 mph traffic speed, our simulations predict TKE of 0.35 m^2/s^2 compared to 0.45 m^2/s^2 predicted by the experimental parameterization. For the 70 mph speed, simulations predict 0.95 m^2/s^2 compared to 0.79 m^2/s^2. It should be noted that the available experimental parameterization is also an approximation, and extrapolation to the present traffic configuration. A more detailed validation of

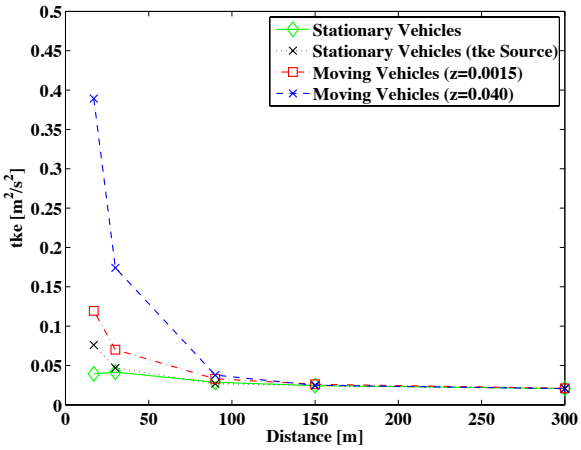

Figure 4. Turbulent kinetic energy (TKE) as a function of distance from highway median for stationary vehicles, stationary vehicles with TKE source (VIT approach), moving vehicles with standard surface roughness (z = 0.0015), and moving vehicles with surface roughness adjusted (z = 0.04) to match TKE predicted by available experimental parameterization [57].

this approach should be performed by comparing predictions with single vehicle measurements in a wind-tunnel configuration.

4.2. Aerosol microphysics in the near-roadway environment

Comparison of simulated and measured CO profiles suggested that accurate predictions of dilution are obtained only when velocity boundary condition is specified on the vehicle surfaces along with adjustment to the vehicle roughness length (z) to account for turbulence generation. Therefore, only this approach is used to perform simulations with multiple selections of aerosol microphysics in the near-roadway environment. However, to investigate the impact of VIM on particle concentration profiles, one simulations was performed with stationary vehicles. The aerosol microphysics model, TOMAS, used in this work has been previously evaluated against dilution tunnel measurements [53] and numerous regional-scale simulations of aerosol microphysics [20, 21, 51, 61]. In this work, the model is used to investigate near-roadway aerosol microphysics with updated OC volatility distribution as discussed previously. Simulations were performed with and without aerosol microphysics to understand the relative impact of dilution and microphysics on aerosol concentration profiles as a function of distance from the roadway. Relative impacts of coagulation and condensation/evaporation were investigated by deactivating the respective microphysics in the model. Also, the Kelvin effect was taken into account for calculation of saturation concentrations of OC2 and OC500. Recently obtained vehicle tailpipe emissions measurements [55, 56] suggest that semi-volatile OC emissions are quite different depending on the vehicle model year and the aftertreatment technology. The gas and particle phase partitioning, and the volatility distribution of OC were also found to be different for different vehicles. For example, as discussed in [55], OC emissions from California LEV-II certified vehicles are lower by an order of magnitude compared to the LEV certified vehicles. Therefore, in order to investigate the sensitivity of aerosol microphysics in the near-roadway environment to tailpipe OC emissions, a simulation was also performed by reducing

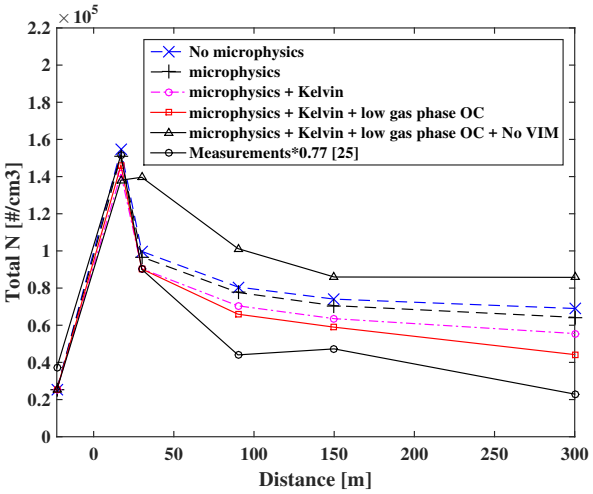

Figure 5. Total particle number concentration (0.65 nm < D_p < 423 nm) as a function of distance from highway median for cases with only dilution (No microphysics), microphysics without Kelvin effect, microphysics + Kelvin effect, microphysics + Kelvin effect + lower gas-phase emissions of OC, and microphysics + Kelvin effect + lower gas-phase emissions of OC but no VIM (stationary vehicles). Available measurements are also shown for reference [26].

the gas-phase OC emissions at the vehicle tailpipes by a factor of 10. While gas-phase OC emissions were reduced by 10 times, emitted number distribution was kept unchanged. This strategy assumes that even in the vehicles fitted with modern emission reduction technology, there always exist very low volatility species that can nucleate. This assumption is supported by measurements of OC emission volatility distribution from diesel and gasoline vehicles [55, 56, 62, 63]. Recent measurements [64] show that a thermal denuder could not completely evaporate fresh traffic emissions even at 400 °C, suggesting the presence of some very low volatility material.

Figure 5 shows total number concentration (0.65 nm < D_p < 423 nm) as a function of distance from the highway median for cases with no microphysics, microphysics without the Kelvin effect, microphysics with the Kelvin effect, and microphysics with the Kelvin effect and low gas-phase emissions of OC with and without VIM. Available measurements are also shown for reference [26]. Since the peak particle concentration in our simulations is slightly different compared to the measurements of [26], the measured data was scaled to match the peak at the 17 m location for the case with microphysics without the Kelvin effect. The first data point corresponds to upwind location, which in the model is at - 20 m (20 m upwind) from the edge of the highway. Particle diameters (D_p) of 0.65 nm and 423 nm represent lower and upper particle size boundaries, respectively, in our model. For all cases, number concentration is highest at the 17 m location followed by rapid dilution to the 30 m location. When VIM is not incorporated in the simulations, particle number concentration is significantly higher compared to all other cases for which VIM was incorporate. Also, comparison with available experimental data suggests that the approach without VIM is not appropriate. Without VIM, rapid dilution near the roadway is not achieved leading to higher particle concentrations for all downwind locations. For the case with no microphysics, particle number concentration decreases from 1.54×10^5 cm^{-3} to about 9.86×10^4 cm^{-3} from 17 m to the 30 m location reflecting a 35%

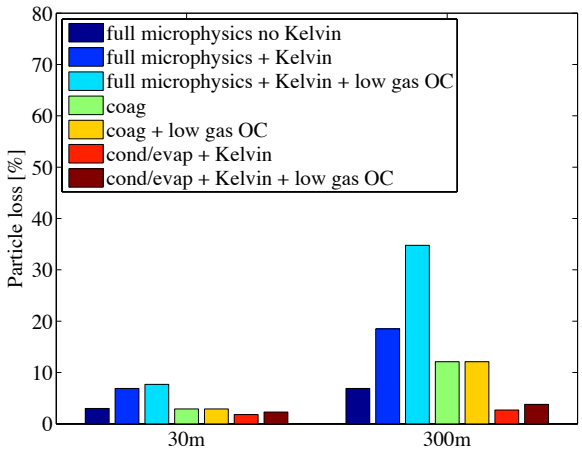

Figure 6. Particle number loss relative to the case with no microphysics at 30 m and 300 m locations for cases with full microphysics without Kelvin effect, full microphysics + Kelvin effect, full microphysics + Kelvin effect + lower gas-phase emissions of OC, only coagulation, only coagulation + lower gas-phase emissions of OC, only condensation/evaporation + Kelvin effect, and only condensation/evaporation + Kelvin effect + lower gas-phase emissions of OC.

reduction, similar to the measurements. The dilution is much more rapid near the roadway due to vehicle-induced mixing as discussed previously for CO emissions. Beyond the 30 m location, the total number concentration is different for each case depending on the type of microphysics activated in the model. When full microphysics (coagulation + condensation/evaporation) is activated in the model, the total number concentration is lower at all downwind locations compared to the case when microphysics was not activated. Overall, all simulation scenarios predict lesser reduction in particle concentration from the 30 m to 300 m location compared to the measurements.

Comparison of simulations with microphysics to the simulation without microphysics provides an indication of particle losses in the near roadway environment. These are better illustrated in Figure 6 which shows particle loss at various locations from the highway median relative to the case with no microphysics. For example, concentration is lower by 3.0%, 3.6%, 4.7%, and 6.9% at locations of 30 m, 90 m, 150 m, and 300 m, respectively, for the case with microphysics, but without accounting for the Kelvin effect. With the Kelvin effect taken into consideration, the loss in particle number is equal to 6.9%, 10.7%, 12.8%, and 18.5% at those four locations. Accounting for the Kelvin effect, therefore, results in a larger particle loss. The largest loss in particle number is, however, achieved for the case with lower gas-phase OC emissions at the tailpipe and the Kelvin effect. For this case, the number concentration is lower by 7.7%, 16.8%, 19.4%, and 35% at the above mentioned locations. It should be mentioned here that the particles are numerically removed from the simulation and considered lost when their diameter becomes smaller than 0.65 nm. For the case with no VIM (not shown in Figure 6), particle concentrations at the sampling height of 1.6 m from the ground, are higher by 44% and 30% at the 30 m and 300 m locations, respectively. Such large difference in particle concentration profiles for the cases with and without VIM strongly suggests that it is important to account for VIM.

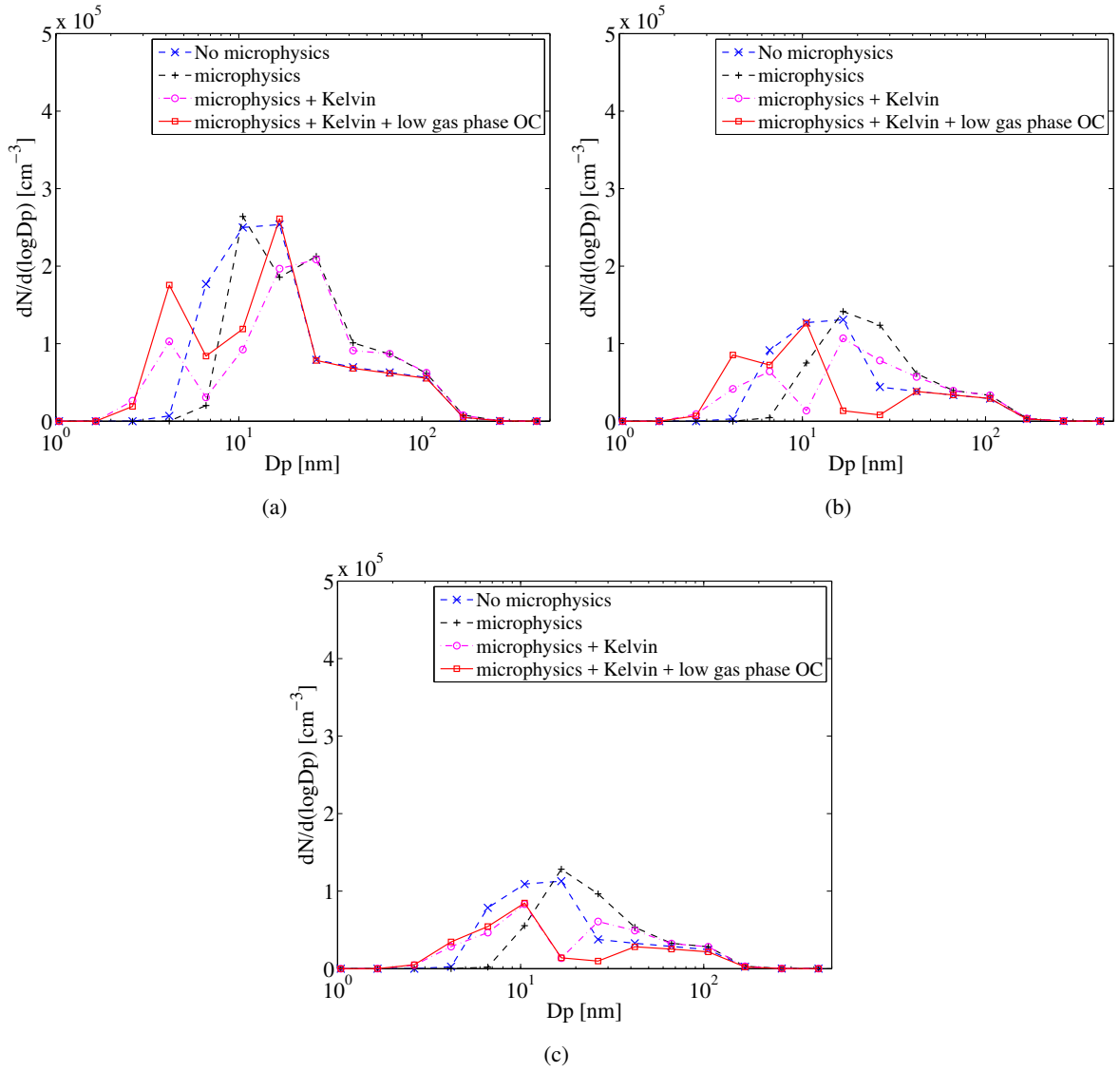

Figure 7. Comparison of particle number distributions for cases with only dilution (No microphysics), microphysics without the Kelvin effect, microphysics + the Kelvin effect, and microphysics + the Kelvin effect + lower gas-phase emissions of OC at the (a) 17 m, (b) 90 m, and (c) 300 m locations.

Figure 7 shows comparison of number distributions at 17 m, 90 m, and 300 m locations, while Figure 8 shows evolution of particle number distribution as a function of distance from highway median for one example case of microphysics with the Kelvin effect. When only dilution is considered in the model, the shape of the number distribution stays unchanged with downwind distance. When microphysics is activated in the model, the number distribution is significantly modified at all locations. At the 17 m location, a growth of particles is observed compared to the case when microphysics was not activated in the model. The mode diameter shifts from 10 nm for the case with no microphysics to 30 nm for the case with microphysics. This growth is primarily due to condensation of OC as

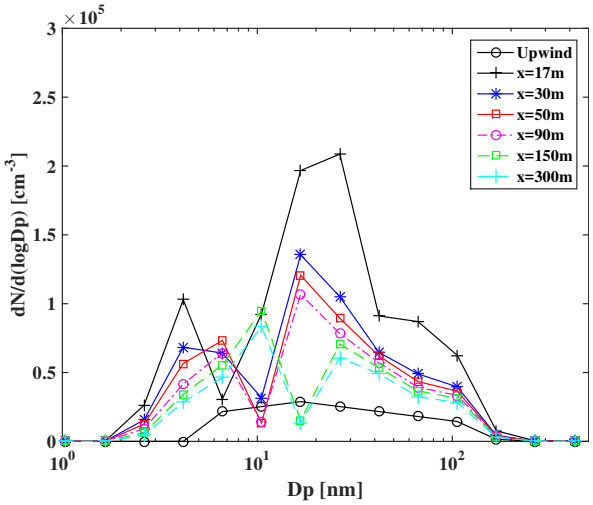

Figure 8. Evolution of particle number distribution as a function of distance from the highway median for case with microphysics + the Kelvin effect.

also reflected in the particle- and gas-phase concentration of OC shown in Figure 9. Figure 9 shows particle- and gas-phase concentrations for the low volatility (C* = 2 μg/m^3) organic component OC2. Concentration profiles for high volatility component (C* = 500 μg/m^3) are not shown as it does not go through a mass transfer between the particle and gas phases. As shown in Figure 9, condensation on the road leads to a considerable increase in particle-phase mass concentration of OC2 from 0.78 μg/m^3 in the background to about 7 μg/m^3 at the 17 m location for the case with higher gas-phase OC emissions. Correspondingly, the gas-phase concentration is lower compared to the cases when microphysics was not activated. Beyond 17 m, distribution starts to shift to lower sizes due to evaporation, and the peak of the distribution now lies near 10 nm particle diameter (Figure 7). As shown in Figure 9, the rate of decrease of gas-phase OC2 concentration becomes lower beyond 90 m location despite atmospheric dilution. This is because dilution of gas-phase OC2 is being partly offset by evaporation of OC2 from particle to gas phase. At the 300 m location, gas-phase concentration of OC2 is 2 μg/m^3 suggesting equilibrium between the particle and gas phases. Accounting for the Kelvin effect leads to slightly higher gas-phase concentration due to a higher effective saturation concentration above the curved surface of the particle. For the case with lower OC emissions at the vehicle tailpipes, the gas-phase concentration actually increases beyond 90 m location. The role of condensation/evaporation in modifying the number distribution in the near-roadway environment has been previously confirmed in experimental [31] and modeling work [25].

Microphysics also affects the concentration of nucleation-mode (D_p < 20 nm), and ultrafine + accumulation-mode ($D_p \geq 20$ nm) particles as shown in Figure 10. Available measurements are also shown for reference [26]. Again, the measurement were re-scaled. Simulations predict a smaller reduction in nucleation-mode particles from the 17 m to the 30 m location compared to the measurements. Concentration of nucleation-mode particles is always largest when microphysics is not activated in the model. When the microphysics is active, the case with lower gas-phase OC emissions has higher concentration of nucleation-mode particles at all distances than the case with higher OC emissions. The difference between the two cases, however, becomes smaller at larger

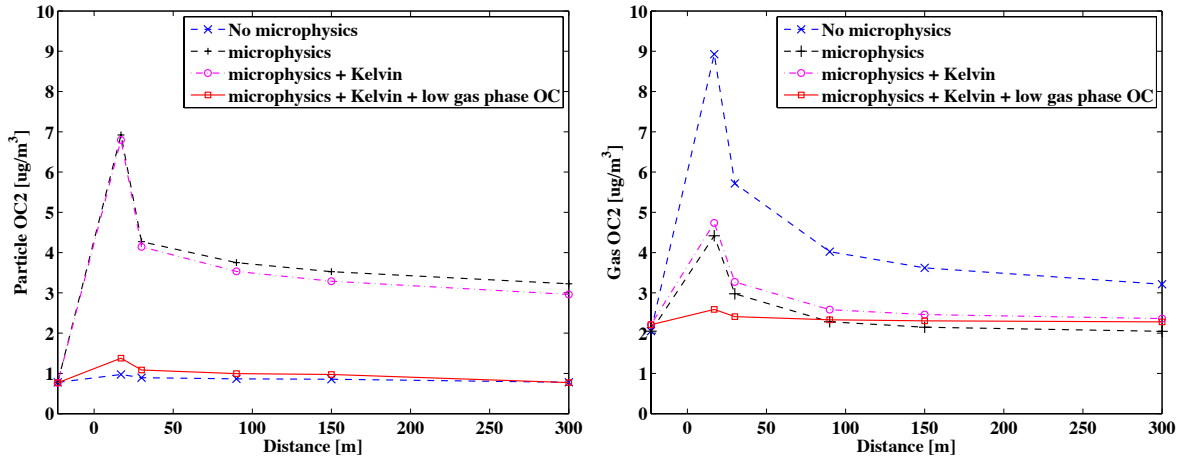

Figure 9. (a) Particle-phase and (b) gas-phase OC2 concentrations as a function of distance from the highway median for cases with only dilution (No microphysics), microphysics without the Kelvin effect, microphysics + the Kelvin effect, and microphysics + the Kelvin effect + lower gas-phase emissions of OC.

distances from the roadway. This is due to combined effect of evaporation and coagulation of smaller particles for the case with lower OC emissions. Concentration of ultrafine and accumulation-mode particles is largest for the case with higher gas-phase emissions of OC. Again, this is due to condensational growth. These results suggest that vehicle technologies that cause a dramatic reduction in gas-phase OC emissions at the tailpipe will likely lead to a higher concentration of nucleation-mode particles in the near-roadway environment (<300 m), assuming that these technologies will not affect the number of newly formed particles at the tailpipe exit. This scenario is plausible if there exists always a critical mass of very low volatility matter at the tailpipe. The low volatility matter can nucleate at the tailpipe exit due to supersaturation, but can later evaporate back into gas-phase due to dilution. There is a large discrepancy between simulations and measurements for accumulation-mode particles. Simulations predict a significant reduction in concentration from 17 m to the 30 m location caused by rapid dilution. The measurements, however, show a slight increase in concentration. This is likely due to a different ratio of nucleation-mode and accumulation-mode particles in simulations and measurements. In our simulations, emissions distributions specified at the vehicle tailpipes lead to almost same number of nucleation-mode and accumulation-mode particles at the 17 m location for the case with microphysics. For measurements, there are almost twice the number of nucleation-mode particles than the accumulation-mode particles. It is likely that the nucleation mode-particles grow to accumulation-mode very rapidly from 17 m to the 30 m location due to combined effect of condensation and coagulation.

In our simulations, loss of particles in the near-roadway environment is due to a combined effect of coagulation and evaporation microphysics. To understand relative roles of coagulation and evaporation on particle loss, simulations were performed by selectively deactivating the condensation/evaporation and coagulation microphysics in the model. It should be mentioned here

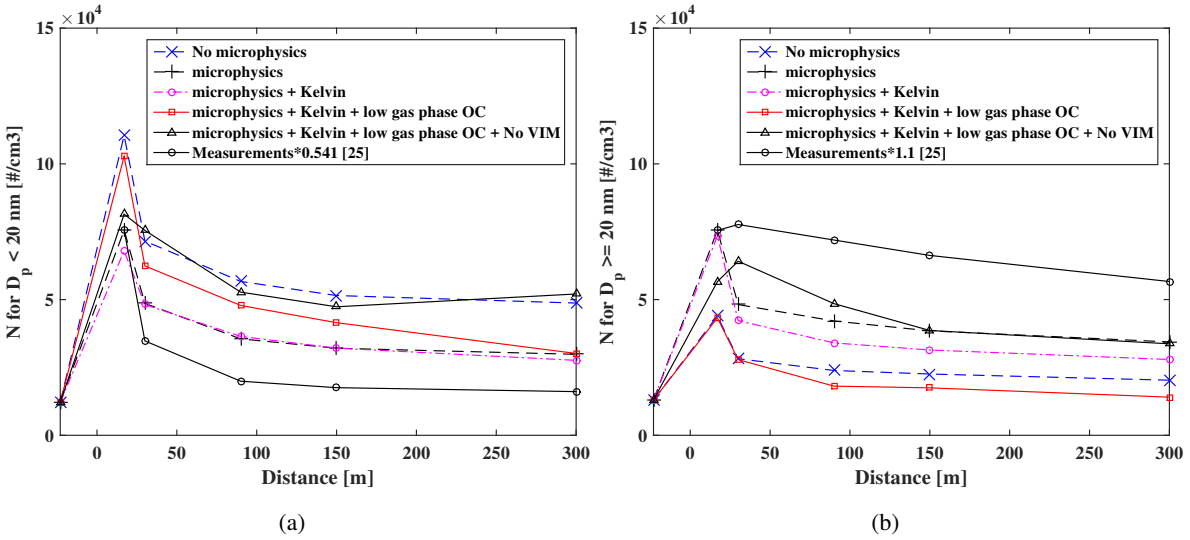

Figure 10. Number concentration of (a) nucleation-mode (D_p < 20 nm) particles and (b) ultrafine + accumulation-mode ($D_p \geq$ 20 nm) particles as a function of distance from the highway median for cases with only dilution (No microphysics), microphysics without the Kelvin effect, microphysics + the Kelvin effect, microphysics + the Kelvin effect + lower gas-phase emissions of OC, and microphysics + Kelvin effect + lower gas-phase emissions of OC but no VIM (stationary vehicles). Available measurements are also shown for reference [26].

that this approach does not precisely separate between the contributions of coagulation and evaporation to particle loss because in reality, both process are coupled and influence each other as discussed later. Figure 6 shows particle loss for various cases relative to the case when microphysics was not considered in the model. To discuss comparative trends among various cases, two locations are considered, the 30 m location which is closer to the roadway, and the 300 m location which is further away from the roadway. As shown in Figure 6, particle loss is highest when full microphysics is activated in the model along with the Kelvin effect and low gas-phase emissions of OC at the tailpipe, and lowest when only condensation/evaporation microphysics is activated. The loss of particles is largest at the 300 m location due to the cumulative effect of evaporation and coagulation along the direction of the wind. The Kelvin effect and gas-phase emissions of OC have significant impact on particle loss. For example at the 300 m location, particle loss increased from 6.9% to 18.5% when the Kelvin effect was included, and to 35% when gas-phase OC emissions at the tailpipe were reduced on top of the Kelvin effect. The particle loss is higher when only coagulation microphysics is activated compared to the case when only condensation/evaporation microphysics is activated. But overall, combined effect of coagulation and condensation/evaporation leads to highest loss of particles. Indeed, evaporation and coagulation compliment each other in removing smaller particles. Figure 11 shows particle number distributions at the 30 m and 300 m locations, respectively, for cases with different selections of microphysics. When only coagulation is activated in the model, the number distribution is narrower compared to when condensation/evaporation microphysics is activated. As shown in Figure 11, evaporation of semi-volatile particles in the 5 nm to 20 nm size range leads to appearance of even smaller particles below 5 nm diameter. These very small particles

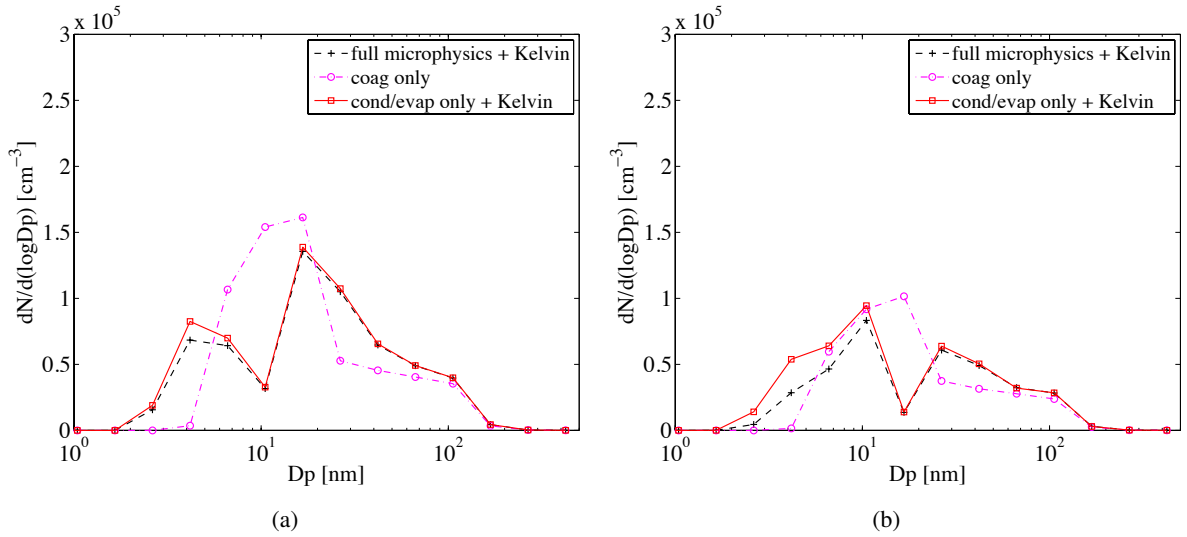

Figure 11. Comparison of particle number distributions for cases with full microphysics + the Kelvin effect, only coagulation, and only condensation/evaporation + the Kelvin effect at the (a) 30 m location and (b) 300 m location.

can now evaporate further or coagulate with larger particles. For the number concentration considered in our simulations, timescale of coagulation of a 3 nm particle with a 100 nm particle is about 1000 seconds. For particles traveling from 30 m to the 300 m location in about 270 seconds, nearly 20% of the 3 nm particles can be lost because of coagulation. Therefore, our simulations suggest that evaporation and coagulation play complementary roles in which evaporation shrinks particles to sizes where they are lost more easily via coagulation. So the coagulation cannot be ignored, especially in a system where very small particles are mixed with larger particles.

5. Conclusions

A Reynolds-Averaged Navier-Stokes (RANS) based turbulent flow solver is coupled with aerosol dynamics equations in the presence of condensation/evaporation and coagulation. Condensation/evaporation of semi-volatile organics is predicted using a two-component volatility basis-set (VBS) model. Simulations are performed to study the dilution and microphysics of traffic-emitted ultrafine particles (UFP) in the near-roadway environment, for up to 300 m from the roadway. Various approaches of simulating vehicle-induced mixing (VIM) are evaluated by comparing the predictions with available experimental parameterization of on-road turbulent kinetic energy generation, and available measurements of CO in the near-roadway environment. Sensitivity simulations were also performed to understand the relative impact of individual microphysical processes, and the impact of tailpipe emissions on near-roadway concentration profiles of UFP.

In order to predict dilution of traffic-emitted pollutants downwind of a roadway, it is important to account for vehicle-induced mixing. However, to fully resolve the velocity boundary layer on the surfaces of moving vehicles, computational mesh requirements are immense, inhibiting a fully resolved simulation even with the RANS type models for turbulent flow. A finer mesh resolution also

leads to a smaller computational timestep size required by numerical stability, further adding to the computational cost. In this work, we have shown that the effect of vehicle-induced mixing can be simulated using a coarse mesh resolution near the vehicle surface by adjusting the vehicle surface roughness parameters. With this approach, it is possible to get good predictions of average turbulent kinetic energy (TKE) generation on the roadway, and vehicle-induced mixing (VIM) of pollutants in the near-roadway environment. Such an approach permits better mesh resolution in the near-road environment while maintaining the computational efficiency of simulations. This approach, however, does not allow for fully coupled simulations of turbulent flow and aerosol microphysics inside the vehicle plume, which is a limitation of the present work. Therefore, it cannot be used to predict nucleation in the exhaust plume, which requires much finer computational mesh and smaller simulation timestep. Another limitation for full-scale microphysics is the lack of reliable nucleation parameterizations. Faster computational techniques and improved nucleation models will be required to span the entire range of turbulent scales and full aerosol microphysics from vehicle tailpipe to the near-roadway environment.

Traffic-emitted aerosol particles are highly dynamic in the near-roadway environment, and predicting their microphysical evolution is challenging due to uncertainty in particle- and gas-phase emissions from vehicles. Better measurements to constrain properties of tailpipe emissions, and to understand downwind evolution of particles are required to further assess model predictions. Our simulations suggest that condensational microphysics dominates particle evolution on the road and in the immediate vicinity (<30 m) of the roadway. Number distribution of emitted EC particles is significantly modified due to condensation of low-volatility organics. As these particles travel away from the roadway, evaporation and coagulation both alter the shape of the distribution, and the result is a net loss of particles. For the number concentrations of UFP considered in our simulations, which are typical of near-roadway environment, timescale for coagulation is relevant for particle removal. For semi-volatile nucleation-mode (D_p < 20 nm) particles, coagulation and evaporation both play complimentary roles in removing smaller particles, especially for particles smaller than 5 nm diameter. Therefore, coagulation cannot be ignored, especially in a system where very small particles are mixed with larger particles. It is also found that the future vehicle technologies targeted at reducing the emissions of low-volatility gas-phase organics, but without reducing the emissions of nucleation-mode particles, might result in higher concentrations of nucleation-mode and lower concentrations of the ultrafine and accumulation-mode particles in the near-roadway environment (<300 m).

Acknowledgments

The authors would like to express their appreciation to Convergent Science Inc. for providing licenses of the CONVERGE code. The authors would also like to thank Dr. Yi Tan of Carnegie Mellon University, and Dr. Jeffrey Pierce of Colorado State University for technical discussion. A portion of the computing time was provided by the National Science Foundation XSEDE program under Grant No. ASC110028 through the Pittsburgh Supercomputing Center (PSC).

Conflict of interest

The authors declare no conflict of interests.

Supplementary

This paper accompanies supplemental information.

References

1. Pope CA, Ezzati M, Dockery DW (2009) Fine-particulate air pollution and life expectancy in the United States. *N Engl J Med* 360: 376–386.
2. Adams PJ, Seinfeld JH (2003) Disproportionate impact of particulate emissions on global cloud condensation nuclei concentrations. *Geophys Res Lett* 30: 335–343.
3. Kanakidou M, Seinfeld JH, Pandis SN, et al. (2005) Organic aerosol and global climate modeling: a review. *Atmos Chem Phys* 5: 1053–1123.
4. Spracklen DV, Carslaw KS, Poschl U, et al. (2011) Global cloud condensation nuclei influenced by carbonaceous combustion aerosol. *Atmos Chem Phys* 11: 9067–9087.
5. Karner AA, Eisinger DS, Niemeier DA (2010) Near-roadway air quality: synthesizing the findings from real-world data. *Environ Sci Technol* 44: 5334–5344.
6. Padro-Martinez LT, Patton AP, Trull JB, et al. (2012) Mobile monitoring of particle number concentration and other traffic-related air pollutants in a near-highway neighborhood over the course of a year. *Atmos Environ* 61: 253–264.
7. Perkins JL, Padro-Martinez LT, Durant JL (2013) Particle number emission factors for an urban highway tunnel. *Atmos Environ* 74: 326–337.
8. Ostro B, Goldberg D, Reynolds P, et al. (2015) Associations of mortality with long-term exposures to fine and ultrafine particles, species and sources: results from the California Teachers Study cohort. *Environ Health Perspect* 123: 549–556.
9. Smith SJ, Bond TC (2014) Two hundred fifty years of aerosols and climate: the end of the age of aerosols. *Atmos Chem Phys* 14: 537–549.
10. Bond TC (2001) Spectral dependence of visible light absorption by carbonaceous particles emitted from coal combustion. *Geophys Res Lett* 28: 4075–4078.
11. Lack DA, Cappa CD (2010) Impact of brown and clear carbon on light absorption enhancement, single scatter albedo and adsorption wavelength dependance of black carbon. *Atmos Chem Phys* 10: 4207–4220.
12. Smith SJ, Mizrahi A (2013) Near-term climate mitigation by short-lived forcers. *Proc Natl Acad Sci* 110: 14202–14206.
13. Dallmann TR, Harley RA, Kirchstetter TW (2011) Effects of diesel particle filter retrofits and accelerated fleet turnover on drayage truck emissions at the Port of Oakland. *Environ Sci Technol* 45: 10773–10779.

14. Dallmann TR, Kirchstetter TW, DeMartini SJ, et al. (2013) Quantifying on-road emissions from gasoline-powered motor vehicles: accounting for the presence of medium- and heavy-duty diesel trucks. *Environ Sci Technol* 47: 13873–13881.
15. May AA, Nguyen NT, Presto AA, et al. (2014) Gas- and particle-phase primary emissions from in-use, on-road gasoline and diesel vehicles. *Atmos Environ* 88: 247–260.
16. Robert MA, Bergen SV, Kleeman MJ, et al. (2007) Size and composition distributions of particulate matter emissions: Part 1 - light-duty gasoline vehicles. *J Air Waste Manage* 57: 1414–1428.
17. Robert MA, Kleeman MJ, Jakober CA (2007) Size and composition distributions of particulate matter emissions: Part 2 - heavy-duty diesel vehicles. *J Air Waste Manage* 57: 1429–1438.
18. Schauer JJ, Kleeman MJ, Cass GR, et al. (1999) Measurement of emissions from air pollution sources. 2. C2 through C30 organic compounds from medium duty diesel trucks. *Environ Sci Technol* 33: 1578–1587.
19. Schauer JJ, Kleeman MJ, Cass GR, et al. (2002). Measurement of emissions from air pollution sources. 5. C1 - C32 organic compounds from gasoline-powered motor vehicles. *Environ Sci Technol* 36: 1169–1180.
20. Adams PJ, Seinfeld JH (2002) Predicting global aerosol size distributions in general circulation models. *J Geophys Res* 107: 4370 – 4392.
21. Pierce JR, Theodoristi G, Adams PJ, et al. (2009) Parameterization of the effect of sub-grid scale aerosol dynamics on aerosol number emission rates. *J Aerosol Sci* 40: 285–293.
22. Sahlodin AM, Sotudeh-Gharebagh R, Zhu Y (2007) Modeling of dispersion near roadways based on the vehicle-induced turbulence concept. *Atmos Environ* 41: 92–102.
23. Wang YJ, Zhang KM (2009) Modeling near-road air quality using a computational fluid dynamics model, CFD-VIT-RIT. *Environ Sci Technol* 43: 7778–7783.
24. Zhang KM, Wexler AS (2004) Evolution of particle number distribution near roadways. part 1: analysis of aerosol dynamics and its implications for engine emission measurements. *Atmos Environ* 38: 6643–6653.
25. Zhang KM, Wexler AS, Zhu YF, et al. (2004) Evolution of particle number distribution near roadways. part ii: the 'road-to-ambient' process. *Atmos Environ* 38: 6655–6665.
26. Zhu YF, Hinds WC, Kim S, et al. (2002) Study of ultrafine particles near a major highway with heavy-duty diesel traffic. *Atmos Environ* 36: 4323–4335.
27. Zhu YF, Hinds WC, Kim S, et al. (2002) Concentration and size distribution of ultrafine particles near a major highway. *J Air Waste Manage Assoc* 52: 1032–1042.
28. Zhu YF, Kuhn T, Mayo P, et al. (2006) Comparison of daytime and nighttime concentration profiles and size distributions of ultrafine particles near a major highway. *Environ Sci Technol* 40: 2531–2536.
29. Zhu YF, Hinds WC, Shen S, et al. (2004) Seasonal trends of concentration and size distribution of ultra fine particles near major highways in los angeles. *Aerosol Sci Tech* 38: 5–13.

30. Huang L, Gong SL, Gordon M, et al. (2014) Aerosol-CFD modelling of ultrafine and black carbon particle emission, dilution, and growth near roadways. *Atmos Chem Phys Discuss* 14: 12235–12278.

31. Biswas S, Ntziachristos L, Moore KF, et al. (2007) Particle volatility in the vicinity of a freeway with heavy-duty diesel traffic. *Atmos Environ* 41: 3479–3493.

32. Salmond JA, Williams DE, Laing G, et al. (2012) The influence of vegetation on the horizontal and vertical distribution of pollutants in a street canyon. *Sci Total Environ* 443: 287–298.

33. Neft I, Scungio M, Culver N, et al. (2016) Simulations of aerosol filtration by vegetation: Validation of existing models with available lab data and application to near-roadway scenario. *Aerosol Sci Tech* 50: 937–946.

34. Salmond JA, Williams DE, Laing G, et al. (2013) The influence of vegetation on the horizontal and vertical distribution of pollutants in a street canyon. *Sci Total Environ* 443: 287–298.

35. Scungio M, Arpino F, Stabile L, et al. (2013) Numerical simulation of ultrafine particle dispersion in urban street canyons with the spalart-allmaras turbulence model. *Aerosol Air Qual Res* 13: 1423–1437.

36. Steffens JT, Wang YJ, Zhang KM (2012) Exploration of effects of a vegetation barrier on particle size distributions in near-road environment. *Atmos Environ* 50: 120–128.

37. Steffens JT, Heist DK, Perry SG, et al. (2013) Modeling the effects of a solid barriers on pollutant dispersion under various atmospheric stability conditions. *Atmos Environ* 69: 76–85.

38. Chang CH, Meroney RN (2003) Concentration and flow distributions in urban street canyons: wind tunnel and computational data. *J Wind Eng Ind Aerod* 91: 1141–1154.

39. Solazzo E, Cai X, Vardoulakis S (2008) Modelling wind flow and vehicle-induced turbulence in urban streets. *Atmos Environ* 42: 4918–4931.

40. Hagler GSW, Tang W, Freeman MJ, et al. (2011) Model evaluation of roadside barrier impact on near-road air pollution. *Atmos Environ* 45: 2522–2530.

41. Hanna SR, Tehranian S, Carissimo B, et al. (2002) Comparisons of model simulations with observations of mean flow and turbulence within simple obstacle arrays . *Atmos Environ* 36: 5067–5079.

42. Gowardhan AA, Pardyjak ER, Senocak I, et al. (2011) A CFD-based wind solver for an urban fast response transport and dispersion model. *Environ Fluid Mech* 11: 439–464.

43. Kota SH, Ying Q, Zhang Y (2013) Simulating near-road reactive dispersion of gaseous air pollutants using a three-dimensional Eulerian model. *Sci Total Environ* 454–455: 348–357.

44. Wang YJ, DenBleyker A, McDonald-Buller E, et al. (2011) Modeling the chemical evolution of nitrogen oxides near roadways. *Atmos Environ* 45: 43–52.

45. Wang YJ, Nguyen MT, Steffens JT, et al. (2013) Modeling multi-scale aerosol dynamics and micro-environment air quality near a large highway intersection using the ctag model. *Sci Total Environ* 443: 375–386.

46. Wang YJ, Zhang KM (2012) Coupled turbulence and aerosol dynamics modeling of vehicle exhaust plumes using the CTAG model. *Atmos Environ* 59: 284–293.

47. Richards K, Senecal P, Pomraning E (2013) *A Three-Dimensional Computational Fluid Dynamics Program for Transient or Steady State Flow with Complex Geometries*. Convergent Science, Inc. Convergent Science, Inc., Middleton,WI (version 2.1.0 ed.).
48. Issa R (1986) Solution of the implicitly discretised fluid flow equations by operator-splitting. *J Comput Phys* 62: 40–65.
49. Tzivion S, Feingold G, Levin Z (1987) An efficient numerical solution to the stochastic collection equation. *J Atmos Sci* 44: 3139–3149.
50. Tzivion S, Feingold G, Levin Z (1989) The evolution of raindrop spectra, part ii, collisional collection/breakup and evaporation in a rainshaft. *J Atmos Sci* 46: 3312–3328.
51. Lee YH, Adams PJ (2012) A fast and efficient version of the two-moment aerosol sectional (TOMAS) global aerosol microphysics model. *Aerosol Sci Tech* 46: 678–689.
52. Shrivastava MK, Stanier CO, Robinson AL (2006) Modeling semi volatile organic aerosol mass emissions from combustion systems. *Environ Sci Technol* 40: 2671–2677.
53. Singh S, Adams PJ, Misquitta A, et al. (2014) Computational analysis of particle nucleation in dilution tunnels: Effects of flow configuration and tunnel geometry. *Aerosol Sci Tech* 48: 638–648.
54. Rader DJ, McMurry PH, Smith S (1987) Evaporation rates of monodispersed organic aerosols in the 0.02- to 0.2-μm-diameter range. *Aerosol Sci Tech* 6: 247–260.
55. May AA, Presto AA, Hennigan CJ, et al. (2013) Gas-particle partitioning of primary organic aerosol emissions: (1) gasoline vehicle exhaust. *Atmos Environ* 77: 128–139.
56. May AA, Presto AA, Hennigan CJ, et al. (2013) Gas-particle partitioning of primary organic aerosol emissions: (2) diesel vehicles. *Environ Sci Technol* 47: 8288–8296.
57. Kalthoff N, Baumer D, Corsmeier U, et al. (2005) Vehicle-induced turbulence near a motorway. *Atmos Environ* 39: 5737–5749.
58. Norris SE, Richards PJ (2011) Appropriate boundary conditions for computational wind engineering models revisited. *J Wind Eng Ind Aerod* 99: 257–266.
59. Zhang KM, Wexler AS, Niemeier DA, et al. (2005) Evolution of particle number distribution near roadways. part iii: traffic analysis and on-road size resolved particulate emission factors. *Atmos Environ* 39: 4155–4166.
60. Lipsky EM, Robinson AL (2005) Design and evaluation of a portable dilution sampling system for measuring fine particle emissions from combustion systems. *Aerosol Sci Tech* 39: 542–553.
61. Jung JG, Pandis SN, Adams PJ (2008) Evaluation of nucleation theories in sulfur-rich environment. *Aerosol Sci Technol* 42: 495–504.
62. Zhao Y, Nguyen NT, Presto AA, et al. (2015) Intermediate volatility organic compound emissions from on-road diesel vehicles: chemical composition, emission factors, and estimated secondary organic aeros production. *Environ Sci Technol* 49: 11516–11526.
63. Zhao Y, Nguyen NT, Presto AA, et al. (2016) Intermediate volatility organic compound emissions from on-road gasoline vehicles and small off-road gasoline engines. *Environ Sci Technol* 50: 4554–4563.

64. Gkatzelis GI, Papanastasiou DK, Florou K, et al. (2016) Measurement of nonvolatile particle number size distribution. *Atmos Meas Tech* 9: 103–114.

© 2018 the Author(s), licensee AIMS Press. This is an open access article distributed under the terms of the Creative Commons Attribution License (http://creativecommons.org/licenses/by/4.0)